River Flow 2010 - Dittrich, Koll, Aberle & Geisenhainer (eds) - © 2010 Bundesanstalt für Wasserbau ISBN 978-3-939230-00-7

Hyperbolicity preserving HLL solver for two-layer shallow-water equations applied to dam-break flows

C. Swartenbroekx, S. Soares-Frazão & B. Spinewine
Fonds National de la Recherche Scientifique & Dept. of Civil and Environmental Engineering, Université catholique de Louvain, B-1348 Louvain-la-Neuve, Belgium

V. Guinot
HydroSciences Montpellier (CNRS, IRD, UM1, UM2), Université Montpellier 2, Montpellier, France

Y. Zech
Dept. of Civil and Environmental Engineering, Université catholique de Louvain, B-1348 Louvain-la-Neuve, Belgium

ABSTRACT: Many types of flows of geophysical interest can be approximated as layered systems made of two shallow fluids of distinct densities. Among these flows, the propagation of a dam-break wave over a granular material can be represented by an upper clear water layer over a dense mixture of water and moving grains. However, the numerical simulation of one-dimensional two-layer immiscible fluid flows has to deal with a number of difficulties. Amongst the challenging difficulties, the 4×4 system of governing equations is known to exhibit a loss of hyperbolicity under certain flow configurations. In this paper, an approximate Riemann solver derived from the Harten-Lax-Van Leer formalism is presented to address the hyperbolicity issue. Numerical results are presented for dam-break flows involving (i) the same fluid upstream and downstream of the dam, (ii) the collapse of a body of light fluid over a uniform layer of a denser fluid, and (iii) a clear-water layer over a granular bed. The results obtained with the new solver are compared to existing experimental data where available.

Keywords: Two-layer model, HLL solver, Hyperbolicity, Dam break, Shallow water

1 INTRODUCTION

In the last decade, two-layer models were developed for a large range of applications in the geophysical flow field, due to the clear physical meaning of the layered flow description. For instance, Zech et al. (2008) discerned the efficiency of a two-layer approach for the simulation of dam-break induced near-field sediment movement, while a classic one-layer model with bank failure operator appeared appropriate only for the far field.

Fraccarollo & Capart (2002) developed a two-layer flow model, in which the upper layer is made of clear water and the lower layer is a mixture of water and sediment, representing a bed-load transport layer. Mass and momentum conservation is imposed separately to each layer while shear-stress closures are imposed between the layers and between the lower layer and the bottom, made of non-moving sediments. In this first model, a same constant sediment concentration and a same constant velocity in the layers were assumed. Capart & Young (2002) relaxed this assumption by decoupling the depth-averaged velocities of the two flowing layers. Spinewine (2005) further considered distinct granular concentrations in the layers and accounted for the granular phase dilatation resulting from grain entrainment across the bed interface. Chen et al. (2007) assumed that the superposed layers differ in velocity, density and also rheology to treat confluence problems, but without considering granular dilatancy. Castro et al. (2007) applied a one-dimensional two-layer model to lock-exchange problems and tested it for the case of the Strait of Gibraltar. Spinewine & Zech (2005) and Chen & Peng (2006) extended the Spinewine (2005) model to two-dimensional configurations. Leal et al. (2006) used the assumption of local equilibrium capacity of sediment transport in a two-layer description, adopting the energy principles of Bagnold to derive different types of closure equations between the layers. Savary & Zech (2007) investigated the boundary conditions and highlighted a possible loss of hyperbolicity of the two-layer model equations (i.e. eigenvalues of the system become complex) under certain conditions. The physical meaning of this loss of hyperbolicity is poorly documented.

In this paper, a modified HLL solver is used. The conservation laws in each layer are written in

a form where most of the coupling between layers is accounted for by specific source terms, thus removing those from the flux terms and hereby preserving strict hyperbolicity of the homogeneous system of equations.

Another difficulty for two-layer models is to balance the source terms induced by interfacial forces, a requirement to avoid spurious interface diffusion and preserve static configurations. Well-balancing is achieved by summing balance equations for the two layers, while a specific procedure is used to prevent spurious interface diffusion.

The present paper presents three applications of the two-layer solver in dam-break configurations. The first considers classical dam-break waves propagating over a fixed bed. The second considers the collapse of a body of light fluid propagating over a uniform layer of a denser fluid. The third considers a dam-break wave propagating over a loose layer of sand. In the latter case, the dense "fluid layer" is made of a mixture of water and moving sediment being entrained by the flood wave; the two-layer solver has consequently been extended to allow for erosion and deposition of sediment.

The paper is organised as follows. The governing equations of the two-layer model are first recalled. The adapted HLL solver accounting for the coupling between the two layers as source terms is then briefly presented. Finally, the three applications are tested and conclusions are drawn.

2 GOVERNING EQUATIONS

The governing equations are developed for two layers of immiscible fluids of distinct densities, using the shallow-water assumption. This means that no mass exchange occurs between the layers. Frictionless motion of the fluid layers is further assumed.

The governing equations can be written in conservation form by means of a continuity and a momentum equation for each layer. As sketched in Figure 1, subscript u denotes the upper layer, usually made of water, or, more generally, of a fluid of lighter density ρ_u and subscript l denotes the lower layer, usually a denser fluid of density ρ_l, for example a mixture of water and sediment.

The continuity equations read

$$\frac{\partial h_k}{\partial t} + \frac{\partial q_k}{\partial x} = 0, \quad k = l, u \tag{1}$$

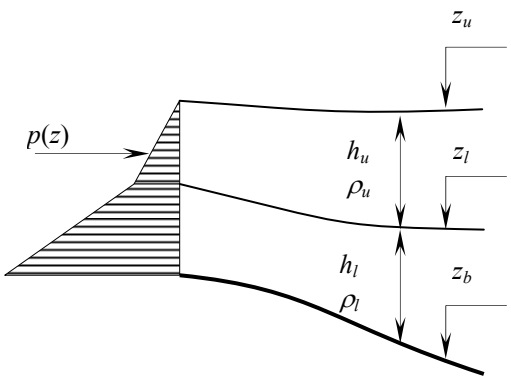

Figure 1. Definition sketch for the flow variables.

where h_k is the depth of the k^{th} layer and $q_k = u_k h_k$ is the unit discharge of layer k (u_k is the depth-averaged velocity of the flow in layer k). The momentum equation for the upper layer u can be written as

$$\frac{\partial q_u}{\partial t} + \frac{\partial}{\partial x}\left(\frac{q_u^2}{h_u} + \frac{g}{2}h_u^2\right) = -gh_u\left(\frac{\partial z_b}{\partial x} + \frac{\partial h_l}{\partial x}\right) \tag{2}$$

where g is the gravitational acceleration and z_b is the bed level. In the same way, the momentum equation for the lower layer l reads

$$\frac{\partial q_l}{\partial t} + \frac{\partial}{\partial x}\left[\frac{q_l^2}{h_l} + \left(\chi h_u + \frac{h_l}{2}\right)gh_l\right] = \chi g h_u \frac{\partial z_l}{\partial x} - g(\chi h_u + h_l)\frac{\partial z_b}{\partial x} \tag{3}$$

where $\chi = \rho_u / \rho_l$ and z_l is the elevation of the interface between the two layers, $z_l = z_b + h_l$. Equations (1), (2) and (3) can be recast in vector conservation form as

$$\frac{\partial \mathbf{U}}{\partial t} + \frac{\partial \mathbf{F}}{\partial x} = \mathbf{S} \tag{4}$$

with vectors **U**, **F** and **S** defined as follows

$$\mathbf{U} = \begin{bmatrix} h_u \\ q_u \\ h_l \\ q_l \end{bmatrix}, \quad \mathbf{F} = \begin{bmatrix} q_u \\ q_u^2/h_u + gh_u^2/2 \\ q_l \\ q_l^2/h_l + gh_l^2/2 + \chi g h_u h_l \end{bmatrix} \tag{5a, b}$$

$$\mathbf{S} = \begin{bmatrix} 0 \\ -gh_u\,\partial z_l/\partial x \\ 0 \\ \chi g h_u\,\partial z_l/\partial x - g(\chi h_u + h_l)\,\partial z_b/\partial x \end{bmatrix} \tag{5c}$$

The Jacobian matrix **A** of system (4) is defined as

$$\mathbf{A}=\frac{\partial \mathbf{F}}{\partial \mathbf{U}}=\begin{bmatrix} 0 & 1 & 0 & 0 \\ c_u^2-u_u^2 & 2u_u & 0 & 0 \\ 0 & 0 & 0 & 1 \\ (c_l')^2\,\chi & 0 & c_l^2-u_l^2 & 2u_l \end{bmatrix} \tag{6}$$

where the celerities c_l , c_u , c'_l, are defined as follows

$$\left.\begin{aligned} c_l^2 &= (h_l+\chi h_u)g \\ c_u^2 &= gh_u \\ (c_l')^2 &= gh_l \end{aligned}\right\} \tag{7}$$

The celerity c_u is the classical celerity of waves in still fluid, while c_l is obtained by transforming the total depth (h_l + h_u) of the upper and lower layers into an equivalent depth ($h_l + \chi\, h_u$). The equivalent depth is defined in such a way that the pressure gradient along a vertical in the upper layer u is the same as in the lower layer l. The quantity c'_l, is introduced only for the convenience of notation. It does not bear any physical meaning such as a wave propagation speed in still fluid. Note that the coupling between the layers appears in the Jacobian matrix **A** only via χ. It is accounted for by the pressure-driven term $-gh_u\partial z_l/\partial x$ in the source term **S**, which comes from the reaction exerted by the lower layer onto the upper layer

As mentioned above, the eigenvalues of **A** are all real and distinct, i.e. this model does not exhibit any loss of hyperbolicity

$$\left.\begin{aligned} \lambda_u^{(1)} &= u_u - c_u \\ \lambda_u^{(2)} &= u_u + c_u \\ \lambda_l^{(1)} &= u_l - c_l \\ \lambda_l^{(2)} &= u_l + c_l \end{aligned}\right\} \tag{8}$$

3 ADAPTED HLL SOLVER

The present section briefly introduces a modified two-layer shallow-water solver.

3.1 *Finite-volume discretisation and principle of the HLL solver*

The governing equations (4) are discretised as follows by a finite-volume scheme with a splitting of source terms derived from the source term upwinding technique (Bermudez & Vazquez-Cendon 1994)

$$\begin{aligned} \mathbf{U}_i^{n+1} &= \mathbf{U}_i^n \\ &+\frac{\Delta t}{\Delta x_i}\left(\mathbf{F}_{i-1/2}^{n+1/2}-\mathbf{F}_{i+1/2}^{n+1/2}\right)+(\mathbf{S}_{i-1/2,i}^{n+1/2}+\mathbf{S}_{i+1/2,i}^{n+1/2})\,\Delta t \end{aligned} \tag{9}$$

where the superscript n denotes the time level n, the subscript i denotes the average value of the variable over the computational cell i, Δt is the computational time step and Δx_i is the length of the cell i. Vectors $\mathbf{S}_{i-1/2,i}^{n+1/2}$ and $\mathbf{S}_{i+1/2,i}^{n+1/2}$ represent the contributions of the source term at the interfaces i – 1/2 and i + 1/2 to the momentum balance in the cell i. The discretisation of the two source terms is detailed in Section 3.2. The flux $\mathbf{F}_{i+1/2}^{n+1/2}$ at the interface i + 1/2 is computed by solving the following local discontinuity problem (Riemann problem)

$$\left.\begin{aligned} &\frac{\partial \mathbf{U}}{\partial t}+\frac{\partial \mathbf{F}}{\partial x}=0 \\ &\mathbf{U}(x,t^n)=\begin{cases}\mathbf{U}_{\mathrm{L}} & \text{for } x < x_{i+1/2} \\ \mathbf{U}_{\mathrm{R}} & \text{for } x > x_{i+1/2}\end{cases} \end{aligned}\right\} \tag{10}$$

where the subscripts L and R denote the value of the variable in the left state and the right state, respectively.

The Riemann problem is not solved exactly, which would require an analytical solution of system (4). An approximate solver, derived from the HLL solver (Harten et al. 1983), is used.

In the original version of the HLL solver, the fluxes are computed assuming that the solution of the Riemann problem is made of two discontinuities separating the left and right state from an intermediate region of constant state (Figure 2). The exact nature of the discontinuities does not need to be known. The jump relationships across the two discontinuities can be solved for the intermediate region of constant state $\mathbf{U}_*$ and $\mathbf{F}_*$

$$\left.\begin{aligned} \mathbf{F}_* &= \frac{\lambda^+\mathbf{F}_{\mathrm{L}}-\lambda^-\mathbf{F}_{\mathrm{R}}}{\lambda^+-\lambda^-}-\frac{\lambda^-\lambda^+}{\lambda^+-\lambda^-}(\mathbf{U}_{\mathrm{L}}-\mathbf{U}_{\mathrm{R}}) \\ \mathbf{U}_* &= \frac{\lambda^+\mathbf{U}_{\mathrm{R}}-\lambda^-\mathbf{U}_{\mathrm{L}}}{\lambda^+-\lambda^-}+\frac{\mathbf{F}_{\mathrm{L}}-\mathbf{F}_{\mathrm{R}}}{\lambda^+-\lambda^-} \end{aligned}\right\} \tag{11}$$

where λ^- and λ^+ denote the propagation speeds of the discontinuities. In the present method, the following estimates, involving (8), are proposed :

$$\left.\begin{aligned} \lambda^- &= \min\left(\lambda_{l,\mathrm{L}}^{(1)},\lambda_{l,\mathrm{R}}^{(1)},\lambda_{u,\mathrm{L}}^{(1)},\lambda_{u,\mathrm{R}}^{(1)},0\right) \\ \lambda^+ &= \max\left(\lambda_{l,\mathrm{L}}^{(2)},\lambda_{l,\mathrm{R}}^{(2)},\lambda_{u,\mathrm{L}}^{(2)},\lambda_{u,\mathrm{R}}^{(2)},0\right) \end{aligned}\right\} \tag{12}$$

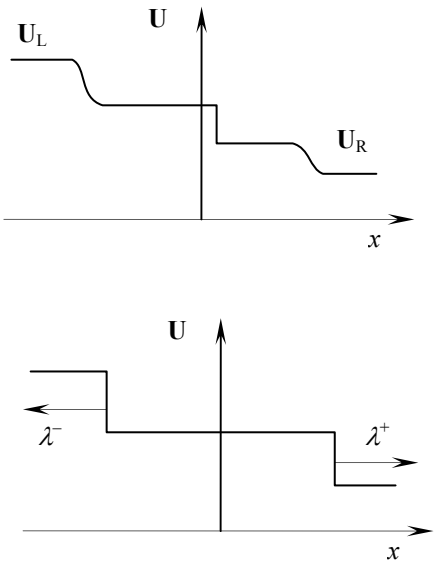

Figure 2. Principle of the HLL Riemann solver. Simplification of the multiple wave exact solution (top) into a two-wave approximate solution (bottom).

3.2 *Discretisation of the source term*

Many approaches for the discretisation of the source terms, involved in equation (9), are available from the literature (see e.g. Gallouët et al. 2003). In the proposed approach, the contributions of the source terms **S** as defined in equation (5c) are discretised as

$$\mathbf{S}_{i+1/2,i}^{n+1/2} = \begin{bmatrix} 0 \\ S_{i+1/2,i}^{(u)} \\ 0 \\ S_{i+1/2,i}^{(l)} \end{bmatrix}, \quad \mathbf{S}_{i+1/2,i+1}^{n+1/2} = \begin{bmatrix} 0 \\ S_{i+1/2,i+1}^{(u)} \\ 0 \\ S_{i+1/2,i+1}^{(l)} \end{bmatrix} \tag{13}$$

where the term $S_{i+1/2,i}^{(k)}$ represents the part of the source term applied to cell i and $S_{i+1/2,i+1}^{(k)}$ is the contribution of the source term to cell $i+1$, with $k = l$ or u. These terms are computed using a classical source term upwinding technique (Bermudez & Vazquez 1994)

$$\left.\begin{aligned} S_{i+1/2,i}^{(k)} &= \frac{\lambda_k^+}{\lambda_k^+ - \lambda_k^-} S_{i+1/2}^{(k)} \\ S_{i+1/2,i+1}^{(k)} &= \frac{-\lambda_k^-}{\lambda_k^+ - \lambda_k^-} S_{i+1/2}^{(k)} \end{aligned}\right\} \tag{14}$$

The wave celerities (12) are used in both layers for the upwinding procedure (13). This guarantees that the second and fourth components of the source term **S** (5c) are assigned in the same way to the cells on both sides of the interface. Consequently, the principle of action and reaction between the two layers is satisfied.

Finally, the source term **S** is computed as

$$\mathbf{S} = \begin{bmatrix} 0 \\ S^{(u)} = g h_{u,LR}(z_{l,\mathrm{L}} - z_{l,\mathrm{R}}) \\ 0 \\ -\chi S^{(u)} + g(\chi h_{u,\mathrm{LR}} + h_{l,\mathrm{LR}})(z_{b,\mathrm{L}} - z_{b,\mathrm{R}}) \end{bmatrix} \tag{15}$$

with

$$h_{k,\mathrm{LR}} = \frac{h_{k,\mathrm{L}} + h_{k,\mathrm{R}}}{2}, \quad k = l, u \tag{16}$$

4 APPLICATIONS

Three dam-break tests are proposed: (i) with water as a single density fluid over a fixed bed, (ii) with a light fluid over a dense fluid over a fixed bed and (iii), with water over an erodible sand bed.

4.1 *Dam-break flow of single density fluid*

Numerical simulations for the propagation of a dam-break wave of pure water are compared to the experimental results obtained by Çağatay & Kocaman (2008) for dry ($\alpha = h_1/h_0 = 0$) and wet bed case ($\alpha = 0.1$ and 0.4), where the initial upstream water depth h_0 is 0.25 m and where the initial downstream tailwater depth is denoted h_1. (Figure 3). In the simulation, it is arbitrarily assumed that $h_u = h_0$ and $h_l = 0$ in the reservoir while $h_u = 0$ and $h_l = h_1$ downstream. So the two bodies of water keep their original identity, while not distinguishable in the reality.

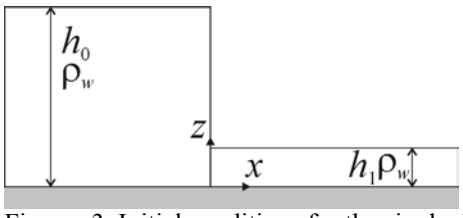

Figures 3. Initial conditions for the single density test.

The dimensionless time T is obtained by multiplying the dimension time t by $(g/h_0)^{1/2}$. Figures 4, 5 and 6 give the water surface profiles at early stages following a dam break. For wet cases (Figures 5 and 6), the grey curve is the contact discontinuity marking the point at which both initially separated fluids are in contact with each other.

For the dry-bed case (Figure 4), the simulated mean slope of the water surface is in good agreement with the experiments and the wave front celerity is slightly underestimated.

For the wet-bed cases (Figures 5 and 6), a negative wave front is propagating upstream while a positive one is observed in the downstream direction. The upstream part is quite well simulated. With the positive wave, a front is forming at early times (Figures 5a and 6a) leading to oscillations and breaking waves at greater times (Figures 5b and 6b). These physical instabilities are not well reproduced by the two-layer model because of the hydrostatic pressure assumption. However the mean level of these waves is well reproduced. The wave front celerity is better simulated for a greater tailwater depth h_1 (Figure 6 in comparison with Figure 5).

4.2 *Dam-break flow of light fluid over dense fluid*

This test aims to investigate different density ratios between the light fluid layer (upper layer *u*) and the denser fluid layer (lower layer *l*). The initial conditions are as sketched in Figure 7. Depending on the density ratio $\chi = \rho_u / \rho_l$, the free-surface will evolve between two asymptotic profiles. For $\chi = 1$, both layers have the same mobility and the free surface will be given by the Dressler solution of a dam-break flow in a channel with an initial tailwater depth, as presented in the previous section. For $\chi = 0$, the top layer will not be able to set the bottom layer in movement, and the Ritter case of a dam-break flow over a fixed, initially dry bed is obtained, where the solution given by Stoker (1957) applies.

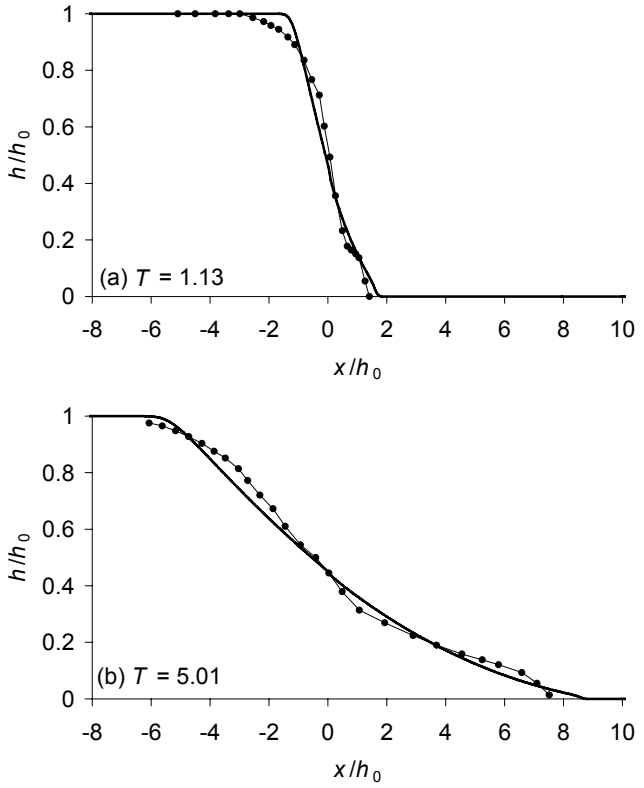

Figure 4. Dam-break flow over dry bed. Computed (black, solid line) and measured (dotted line) water surface profiles at time (a) $T = 1.13$, (b) $T = 5.01$.

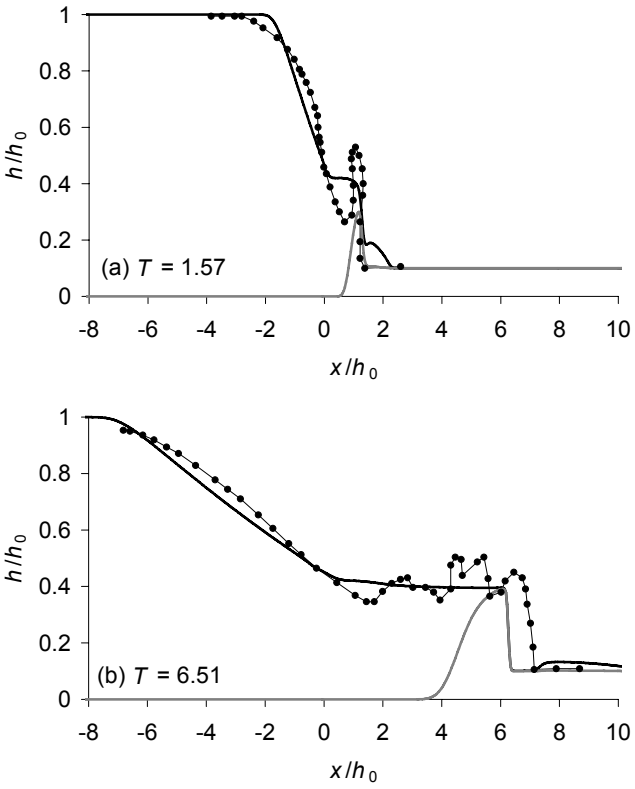

Figure 5. Dam-break flow over wet bed ($\alpha = 0.1$). Computed (black, solid line) and measured (dotted line) water surface profiles at time (a) $T = 1.57$, (b) $T = 6.51$. Grey line: contact discontinuity between reservoir and tailwater.

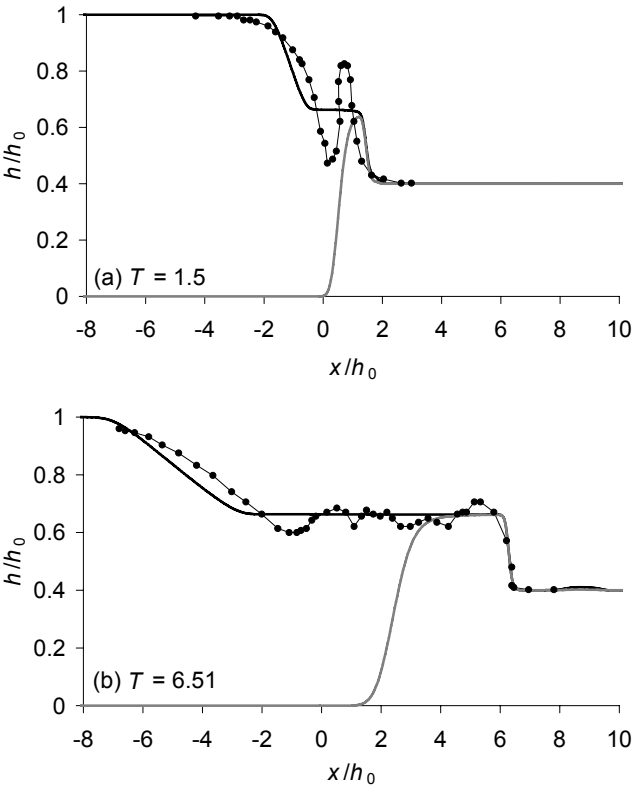

Figure 6. Dam-break flow over wet bed ($\alpha = 0.4$).Computed (black solid line) and measured (dotted line) water surface profiles at time (a) $T = 1.5$, (b) $T = 6.51$. Grey line: contact discontinuity between reservoir and tailwater.

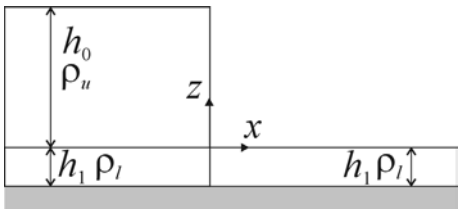

Figure 7. Initial conditions for the light fluid over dense fluid test case.

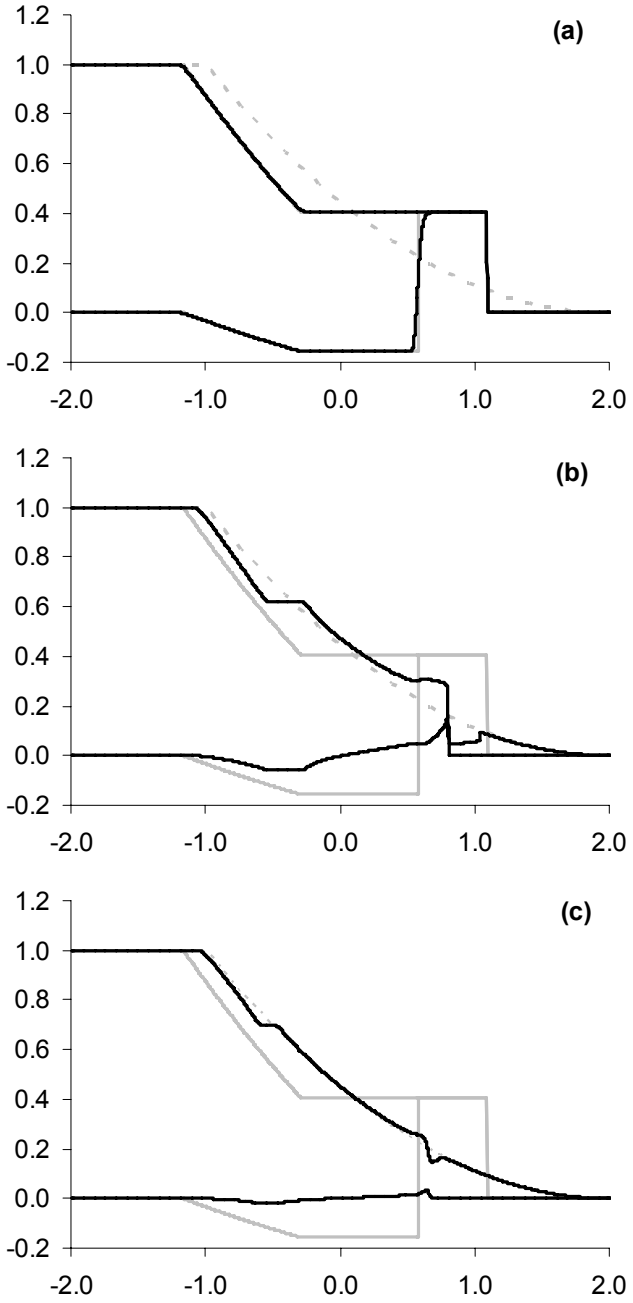

Figure 8. Dam-break flow of a light fluid over a dense fluid (a) $\chi = 1$, (b) $\chi = 0.2$ and (c) $\chi = 0.05$. Abscissa: $x / (gh_0)^{1/2}$, ordinate: h / h_0. Solid black lines: numerical solution. Solid grey lines: limit case for $\chi = 1$ (Dressler solution). Dashed grey lines: limit case for $\chi = 0$ (Ritter solution).

Figure 8 shows the computed results for the following density ratios: (a) $\chi = 1$, (b) $\chi = 0.2$ and (c) $\chi = 0.05$. They are given for a non-dimensional time $T = 2500$. The depths h_0 and h_1 are 1 m and 0.357 m, respectively. In each figure, the two asymptotic profiles are indicated in light grey. The evolution from the Dressler / Stoker solution to the Ritter / Stoker (Stoker 1957) solution can be clearly observed for decreasing density ratios. Interesting to note is also the small wave propagating ahead of the main front that progressively evolves towards the classical shape of a dam-break wave front over dry bed, where the free surface is tangent to the bottom. This is referred to as a "Ritter pinch-off" by Spinewine (2005).

4.3 *Dam-break flow over granular bed*

This test studies the morphological evolution of a moving sediment layer (transport or bottom layer *s*) under the action of a water flow (top layer *w*). In particular, this test aims to reproduce the laboratory results of small-scale dam-break waves on an initially flat sand bed obtained by Spinewine & Zech (2007). In this case, the bottom boundary is made of a loose sand layer which is allowed to erode or deposit. In the following, the top level z_u becomes z_w, the clear-water level, z_l becomes z_s, the upper level of the transport layer and, z_b is the movable bed level (Figure 9).

In order to account for the bed erodibility, the physical and numerical model presented in Sections 2 and 3 is extended following Spinewine (2005) and Savary (2007). The hypotheses of immiscible and frictionless fluids are no valid anymore. Indeed, mass and momentum transfer may occur between the layers, due to the change in sediment concentration (C_b, C_s) and velocities ($u_b = 0$, u_s, u_w). Granular dilatancy is considered, i.e. the mobilization of bed material is associated with an expansion of the granular matrix so that the volumetric sediment concentration in the moving layer is lower than in the static bed (transition from solid-like to fluid-like behaviour). For instance, in case of erosion, sediments from the bed are incorporated in the transport layer and, to recover a constant sediment concentration in the transport layer, water is leaving the clear-water layer to enter the transport layer. The transport layer depth is thus increasing while the clear-water layer depth is diminishing and the bed level is lowered. From the point of view of the clear-water layer, there is a loss of mass, but also a loss of momentum associated with water leaving the clear-water layer at velocity u_w to enter the transport layer at velocity u_s. Moreover, diffusive momentum transfers occur due to friction at the interface between the layers.

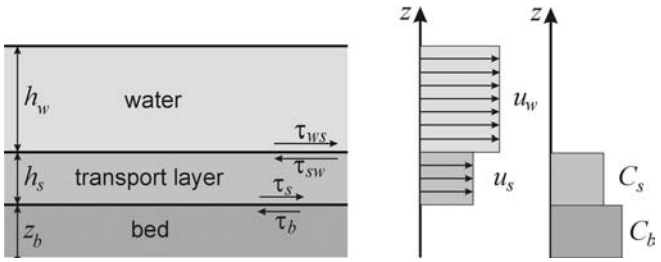

Figure 9. Two-layer model with a moving sediment layer.

The definition of an erosion rate e_b is thus added to the system of governing equations. This erosion rate is the evolution of the interface level with time $-\partial z_b/\partial t$, due to vertical sediment transfer between the bed and the transport layer. It is positive in case of erosion. In a similar way, the rate e_s, related to the displacement of interface $-\partial z_s/\partial t$ is defined and can be related to e_b.

Three source terms are also added to the governing equations: they express (i) geomorphic interactions between the layers (involving the interface displacement rates e_b and e_s), i.e. mass and convective momentum transfer, (ii) friction at the interface between the water layer and the transport layer (involving the shear stress exerted by water on the transport layer τ_{ws}) and, (iii) friction at the interface between the transport layer and the bed (involving the resistance shear stress to the flow exerted by the bed τ_b).

The modification of system (4) becomes

$$\frac{\partial h_w}{\partial t}+\frac{\partial q_w}{\partial x}=e_s \tag{17a}$$

$$\frac{\partial h_s}{\partial t}+\frac{\partial q_s}{\partial x}=e_b-e_s \tag{17b}$$

$$\frac{\partial q_w}{\partial t}+\frac{\partial}{\partial x}\left(\frac{q_w^2}{h_w}+\frac{g}{2}h_w^2\right) = -gh_w\left(\frac{\partial z_b}{\partial x}+\frac{\partial h_s}{\partial x}\right)+u_w e_s-\frac{\tau_{ws}}{\rho_w} \tag{17c}$$

$$\frac{\partial q_s}{\partial t}+\frac{\partial}{\partial x}\left[\frac{q_s^2}{h_l}+\left(\chi h_w+\frac{h_s}{2}\right)gh_s\right] = \chi g h_w\frac{\partial z_s}{\partial x}-g(\chi h_w+h_s)\frac{\partial z_b}{\partial x}-\chi u_w e_s+\frac{\tau_{ws}}{\rho_s}-\frac{\tau_b}{\rho_s} \tag{17d}$$

$$\frac{\partial z_b}{\partial t}=-e_b \tag{17e}$$

with the displacement rates given by

$$e_b=\frac{\tau_s-\tau_b}{\rho_b u_s} \tag{18}$$

$$e_s=-\frac{C_b-C_s}{C_s}e_b \tag{19}$$

and with the shear stresses

$$\tau_{ws}=\rho_w C_{fw}\left|u_w-u_s\right|\left(u_w-u_s\right) \tag{20a}$$

$$\tau_s=\rho_s C_{fs}\left|u_s\right|\left(u_s\right) \tag{20b}$$

$$\tau_b=\tau_{crit}+tg\varphi\left(\rho_s-\rho_w\right)g h_s \tag{20c}$$

where ρ_w, ρ_s and ρ_b are the water, transport layer and bed volumetric mass, respectively, C_{fw} and C_{fs} the water and sediment friction coefficients, τ_{crit} the threshold value of τ_b allowing for erosion and φ the angle of repose. The following values are adopted (Spinewine 2005): $\rho_w = 1000$ kg/m³, $\rho_s = 1369.6$ kg/m³, $\rho_b = 1890.4$ kg/m³, $C_s = 0.22$, $C_b = 0.53$, $C_{fw} = 0.008$, $C_{fs} = 0.06$, $\tau_{crit} = 0$ and $\varphi = 30°$.

Figure 10 shows the simulated and experimental levels for the early times of a dam-break with a initial water level h_{w0} of 0.35 m in the reservoir and an initial flat bed at $z_b = 0$ m. Although the general trend is well reproduced by the model, the simulated wave front celerity is overestimated and

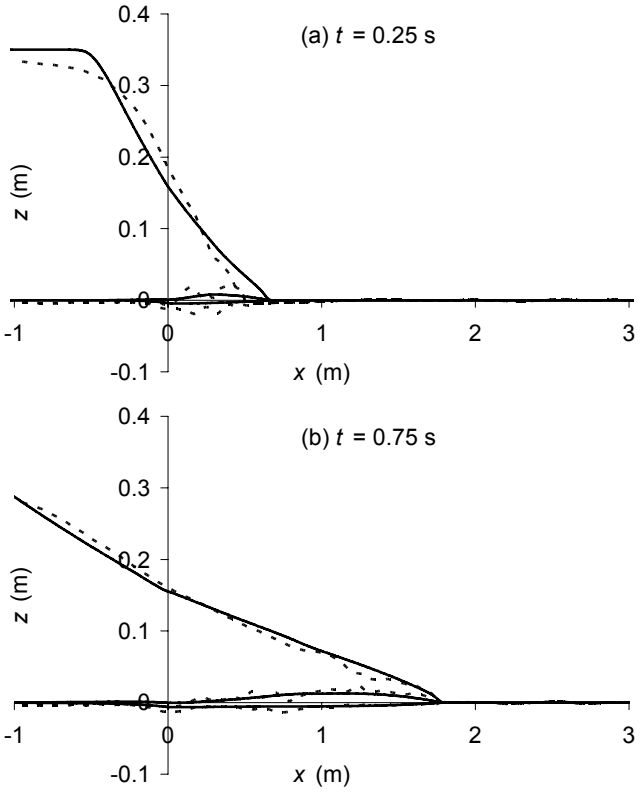

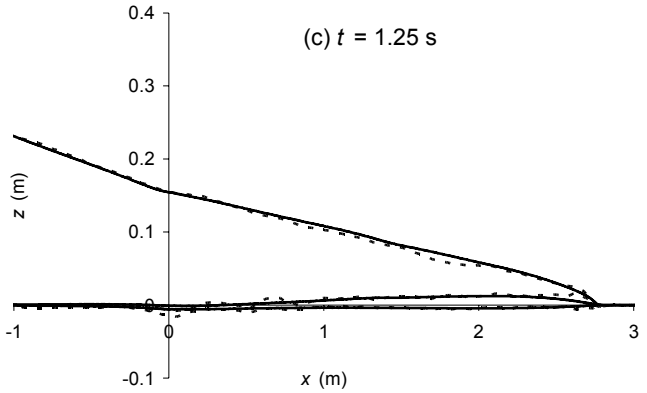

Figure 10. Dam-break wave over mobile bed, simulated (solid line) and experimental (dashed line). From up to down water, transport and bed levels.

the transport layer depth h_s is underestimated at the earliest time (Figure 10a).

5 CONCLUSION

Two-layer models may be useful when two bodies of fluids interact, for instance in case of dam-break over mobile bed. In the literature, one of the main problems associated with two-layer models is the loss of hyperbolicity that occurs under certain flow configurations (Savary & Zech 2007). This is due to the interactions between the two fluid layers.

This paper described an adapted HLL solver to face this difficulty. Including the pressure-induced terms in the source terms allows the loss of hyperbolicity to be avoided. Three dam-break applications are tested. The first one consists in a single density fluid, namely water, propagation over fixed bed in dry and wet conditions. The second test treats a light fluid over a denser fluid. These two first cases assume immiscible and frictionless fluids. A third application shows the possibility for the model to treat mobile-bed cases, if frictional and geomorphic source terms are added to the system, allowing erosion and deposition of bed sediment.

These applications give good confidence for further research in the dam-break simulation with two-layer shallow-flow models. Some possible improvements could be explored: relaxed assumptions about velocity distribution in the layers, numerical second-order accuracy developments, and a two-dimensional extension of the presented model.

ACKNOWLEDGEMENTS

The present work was funded by a joint mobility grant from CNRS/FNRS-FRS-CGRI, n° 20183 “Modèles bicouches d’écoulement sur lit mobile”. The experimental data discussed in section 4.1 were kindly made available by Prof. H. Çağatay and S. Kocaman, from the Hydraulic Laboratory at the Civil Engineering Department of Çukurova University, Turkey.

REFERENCES

Bermudez, A., Vazquez-Cendon, M.E. 1994. Upwind methods for hyperbolic conservation laws with source terms. Computers & Fluids, 23(8), 1049–1071.

Çağatay, H., Kocaman, S. 2008. Experimental study of tail-water level effects on dam break flood wave propagation. Proceedings River Flow 2008, Altinakar, M. et al. (eds.), Çeşme, Turkey, 635-644.

Capart, H., Young, D.L. 2002. Two-layer shallow water computations of torrential geomorphic flows. Proceedings River Flow 2002, Bousmar, D. & Zech, Y. (eds.), Louvain-la-Neuve, Belgium, 1003–1012.

Castro, M.J., García-Rodríguez, J.A., González-Vida, J.M., Marcías, J., Parés, C. 2007. Improved FVM for two-layer shallow-water models: Application to the Strait of Gibraltar. Advances in Engineering Software. 38, 386-398.

Chen, S.-C., Peng, S.-H. 2006. Two-dimensional numerical model of two-layer shallow water equations for confluence simulation. Advances in Water Resources, 29, 1608-1617.

Chen, S.C., Peng, S.H., Capart, H. 2007. Two-layer shallow water computation of mud flow intrusions into quiescent water. Journal of Hydraulic Research, 45(1), 13–25.

Fraccarollo, L., Capart, H. 2002. Riemann wave description of erosional dam-break flows. Journal of Fluid Mechanics, 461, 183 – 228.

Gallouët, T., Hérard, J.M., Seguin, N. 2003. Some approximate Godunov schemes to compute shallow-water equations with topography. Computers & Fluids, 32, 479–513.

Harten, A., Lax, P., Van Leer, B. 1983. On upstream differencing and Godunov-type schemes for hyperbolic conservation laws. Journal of Computational Physics; 50, 235–269.

Leal, J.G.A.B., Ferreira, R.M.L., Cardoso, A.H. 2006. Dam-break wave-front celerity. Journal of Hydraulic Engineering, ASCE, 132(1), 69-76.

LeVeque, R.J. 2002. Finite-Volume Methods for Hyperbolic Problems. Cambridge University Press.

Savary, C. 2007. Transcritical transient flow over mobile bed. Two-layer shallow-water model. PhD thesis, Université catholique de Louvain.

Savary, C., Zech, Y. 2007. Boundary conditions in a two-layer geomorphological model. Application to a hydraulic jump over a mobile bed. Journal of Hydraulic Research, 45(3), 316–332.

Spinewine, B. 2005. Two-layer flow behaviour and the effects of granular dilatancy in dam-break induced sheet-flow. PhD thesis, Université catholique de Louvain.

Spinewine, B., Zech, Y. 2005. Dam-break on a movable bed in presence of an initial bed discontinuity: laboratory experiments and simulations with a multi-layer shallow water model. Proceedings 31st IAHR Congress, Seoul, Korea, 3422-3433.

Spinewine, B., Zech, Y. 2007. Small-scale laboratory dam-break waves on movable beds. Journal of Hydraulic Research, IAHR, 45 Extra Issue, 73-86.

Stoker, J.J. 1957. Water Waves. Wiley.

Bermudez A., Vazquez-Cendon M.E. 1994. Upwind methods for hyperbolic conservation laws with source terms. Computers & Fluids, 23, 1049–1071.

Zech, Y., Soares-Frazão, S., Spinewine, B., le Grelle, N. 2008. Dam-break induced sediment movement: Experimental approaches and numerical modeling. Journal of Hydraulic Research, IAHR, 46 (2), 176-190.